Heliyon

ELSEVIER

Received:
15 June 2018
Revised:
30 August 2018
Accepted:
20 September 2018

Cite as: Xinyu Tan, Mingzhi Luo, Allen P. Liu. Clathrin-mediated endocytosis regulates fMLP-mediated neutrophil polarization. Heliyon 4 (2018) e00819. doi: 10.1016/j.heliyon.2018.e00819

Clathrin-mediated endocytosis regulates fMLP-mediated neutrophil polarization

Xinyu Tan [a,1], **Mingzhi Luo** [a,b], **Allen P. Liu** [a,c,d,e,*]

[a] *Department of Mechanical Engineering, University of Michigan, Ann Arbor, Michigan, United States*

[b] *Institute of Biomedical Engineering and Health Sciences, Changzhou University, Changzhou, Jiangsu, PR China*

[c] *Department of Biomedical Engineering, University of Michigan, Ann Arbor, Michigan, United States*

[d] *Cellular and Molecular Biology Program, University of Michigan, Ann Arbor, Michigan, United States*

[e] *Biophysics Program, University of Michigan, Ann Arbor, Michigan, United States*

[*] Corresponding author.

E-mail address: allenliu@umich.edu (A.P. Liu).

[1] Present address: CareEvolution, Ann Arbor, Michigan, United States.

Abstract

A cell's ability to establish polarization is one of the key steps in directional migration. Upon the addition of a chemoattractant, N-formylmethionyl-leucyl-phenylalanine (fMLP), neutrophils rapidly develop a front end marked by a wide and dense actin network which is a feature of cell polarization. Despite a general understanding of bi-directional crosstalk between endocytosis and polarization, it remains unclear how clathrin-mediated endocytosis (CME) induced by chemoattractant binding to formyl peptide receptor (FPR) affects neutrophil polarization. In this work, we characterized the spatial organization of FPR and clathrin-coated pits (CCPs), the functional unit of CME, with and without fMLP and found that fMLP induced different distributions of FPR and CCPs. We further found that cells had impaired polarization induced by fMLP when CME is inhibited by small molecule inhibitors. Under these conditions, pERK, $pAkt_{308}$, and $pAkt_{473}$ were all severely blocked or had altered dynamics. The spatial organization between actin and two major clathrin-mediated endocytic proteins, clathrin and β-arrestin, were distinct and supported clathrin and β-arrestin's functional roles in mediating neutrophil polarization. Together these

https://doi.org/10.1016/j.heliyon.2018.e00819

results suggest that CME plays a pivotal role in a complex process such as cell polarization.

Keyword: Cell biology

1. Introduction

Within tens of seconds to several minutes upon binding of N-formylmethionyl-leucyl-phenylalanine (fMLP) to formyl peptide receptors (FPR), neutrophils rapidly establish polarity, with lamellipodia protruding in the front and a long tail at the back. Many molecular effectors involved in this process are known [1], including the ones that mediate G protein and arrestin signaling [2]. Like most G protein-coupled receptors (GPCRs), agonist binding to FPR triggers receptor internalization from the plasma membrane to intracellular compartments [3]. Although bi-directional interplay between signal transduction and endocytosis is an emerging theme [4, 5], the interplay between fMLP-FPR signaling in the context of neutrophil polarization and endocytosis has not been investigated in detail.

Clathrin-mediated endocytosis (CME) is one of the major endocytic pathways that GPCRs are internalized following ligand binding [6]. CME has been shown to play an important role in signal transduction mediated by GPCRs. It actively regulates the turnover of the receptors on the membrane, thereby governs the amount of signal a cell can receive. CME occurs through the assembly of discrete clathrin-coated pits (CCPs), and each is a macromolecular assembly that consists of scaffold/signaling molecules such as β-arrestin [2]. Many studies have shown the importance of CME in the establishment of cell polarization. For example, in polarized budding yeast, endocytotic vesicles corral central exocytic zone to establish robust polarity [7]. In migrating cells, the spatial distribution of CCPs has been a subject of debate. Early electron microscopy studies showed that CCPs appeared to be at the back and almost none at the front lamellipodia [8]. However, another study observed that CCPs were polarized at the leading edge in migrating Madine Darby canine kidney (MDCK) cells [9]. Using spinning-disk confocal microscopy and lattice light-sheet microscopy, Kural *et al.* characterized CCP distribution in migrating glioblastoma cells and found spatial differences in CCP dynamics between dorsal and ventral membrane [10].

In the present work, we aim to investigate the role of CME during the polarization of HL-60-derived neutrophil (hereafter referred to as neutrophil). We first quantified the spatial co-distribution of FPR and CCP in fMLP-stimulated and non-stimulated neutrophils. The phenotype differences in polarization for fMLP-stimulated and non-stimulated cells suggested that CME might be important in neutrophil polarization. We further demonstrated the importance of CME for

https://doi.org/10.1016/j.heliyon.2018.e00819

effective polarization using high content imaging and pharmacological perturbation of clathrin and dynamin. Both treatments potently blocked neutrophil polarization and fMLP-induced ERK and Akt signaling. Analysis of actin-clathrin and actin-β-arrestin spatial correlation revealed differential interaction between actin cytoskeleton and endocytic proteins with and without fMLP, suggesting a close-knit relationship between CME and FPR signaling during neutrophil polarization.

2. Results and discussion

2.1. CCPs and FPR spots organize differently in the presence of fMLP

To investigate the spatial organization between FPRs and CCPs, we imaged FPRs and CCPs in fixed HL-60 derived neutrophils using total internal reflection fluorescence microscopy (TIR-FM) without and with uniform 100 nM fMLP after 5 minutes. In a uniform concentration of fMLP, neutrophils start to polarize with distinctive phenotypes, such as a dramatic increase in cell area, adopting an elongated shape, and formation of polarized signaling molecules and sub-cellular structures within the cell. TIR-FM microscopy uses a thin evanescent excitation field to observe the ventral cell surface, and largely avoids fluorescence signals from intracellular structures. Besides a significant increase in cell size, we observed more FPR and CCP puncta and a noticeable greater degree of colocalization in fMLP-treated cells (Fig. 1A). Using Pearson correlation coefficient, a standard colocalization analysis, between the two fluorescence channels, there was a large variation and an overall smaller mean Pearson correlation coefficient for fMLP-treated cells (Fig. 1B). However, this metric only measures the linear relationship between two variables and ignores local structures of the data; therefore, a more detailed analysis is needed.

To investigate this further, CCPs and FPRs puncta were detected using point-source detection software package based on an improved Gaussian mixture model [11]. We noticed that there was a dramatic increase in the number of CCPs and FPR puncta upon fMLP stimulation and there were more FPR puncta than CCPs under both stimulating and non-stimulating conditions. However, not all of the CCPs were associated with FPRs, where we defined the association by the number of FPRs within a 5-pixel (~290 nm) radius of a CCP. There were ~17.3% of CCPs without FPRs nearby (vacant CCPs) for the control condition compared to ~10.6% for the fMLP-treated condition (Fig. 1C). In addition, there were significantly more CCPs with FPRs (occupied CCPs) in the fMLP-treated condition. We next asked whether the increased number of CCPs and FPRs were scattered randomly on the membrane with uniformly distributed intensity and how many FPR puncta were around a CCP. To provide a more comprehensive view of the data, we mapped each individual CCP to a plane where *x*-axis is the CCP intensity and *y*-axis is the number of FPR puncta

https://doi.org/10.1016/j.heliyon.2018.e00819

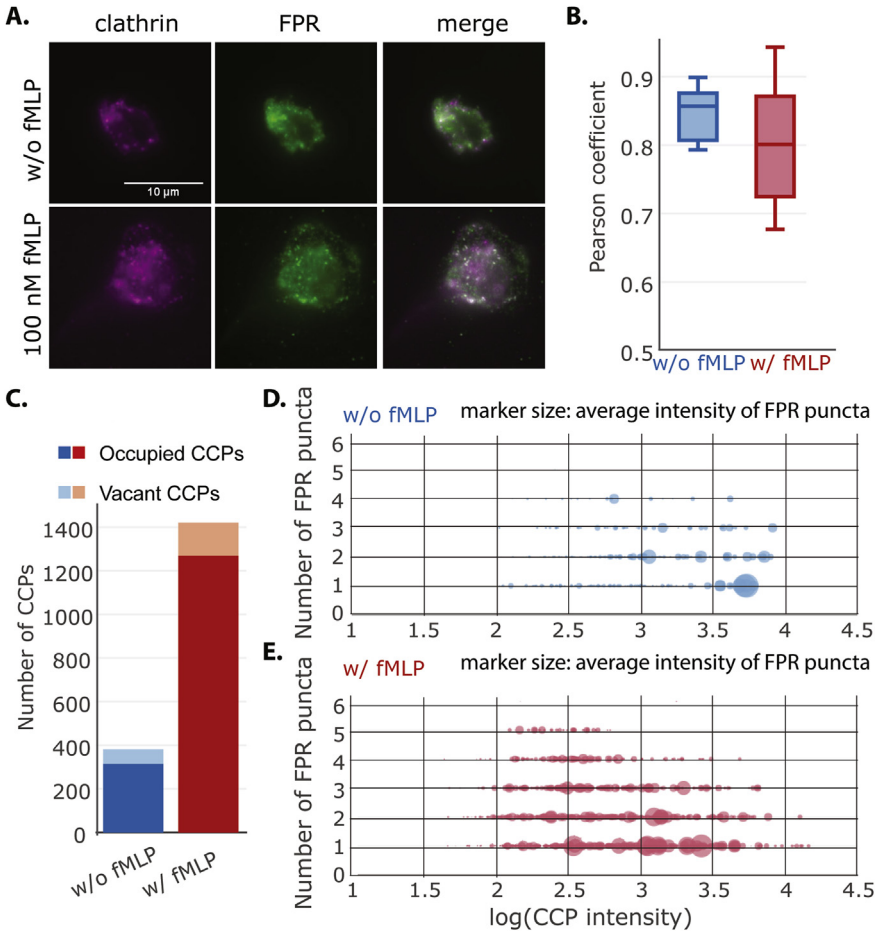

Fig. 1. Spatial organizations between CCPs and FPRs are different with and without fMLP. (A) Example TIRF images of FPR (green) and CCP (magenta) without (upper) and with (bottom) 100 nM fMLP. (B) Pixel-wise Pearson coefficient was quantified. Wilcoxon rank-sum test $p = 0.46$ does not reject the null hypothesis. ($n_{w/o\ fMLP} = 8$, $n_{fMLP} = 8$) (C) The bar graph of the number of occupied CCPs and vacant CCPs, where we define 'vacant CCPs' as CCPs without FPR spots within its 10-pixel radius. (Occupied CCP number: $n_{w/o\ fMLP} = 315$, $n_{fMLP} = 1270$; vacant CCP number: $n_{w/o\ fMLP} = 66$, $n_{fMLP} = 151$; a total of 8 cells were analyzed in each condition) (D) Scatter plot of CCP intensity (in log scale) *vs.* number of FPR spots. Each dot in the plot represents a CCP with its *x*-axis representing its intensity and *y*-axis the number of FPR spots nearby (where we define 'nearby' as the distance within a 10-pixel radius). The size of the dot represents the average intensity of all the FPR spots nearby. Only occupied CCPs were included in these two plots. (Occupied CCP number: $n_{w/o\ fMLP} = 315$, $n_{fMLP} = 1270$).

surrounding it with the marker size indicating the FPR intensity (Fig. 1D and E). From the two scatter plots, it is apparent that the plot for non-stimulation is not a down-sampled version of the plot for fMLP-stimulated condition. Rather, the two conditions had distinct distributions in the three variables presented. In the presence of fMLP, the increase in CCP numbers was not uniform against CCP intensity – there were much more dimmer (*i.e.*, log(CCP intensity) < 3) structures than the brighter ones. Interestingly, it is the dimmer CCP structures where we found more surrounding FPR puncta as well as more FPRs (*i.e.,* larger circles). While the

https://doi.org/10.1016/j.heliyon.2018.e00819

increase in dimmer structures could due to a greater z distance from the imaging plane, fMLP treatment increases neutrophil spreading and this should provide an overall greater attachment to the substrate. The increase in FPR in dimmer CCPs is similar to a finding reported recently that short-lived (*i.e.,* dim CCPs) have more epidermal growth factor receptors (EGFR) [12]. This is also consistent with cargo clustering that nucleate *de novo* CCPs [13]. Altogether, the above results demonstrated that fMLP stimulation led to an interaction between FPR and CCPs and thus CME is responsive to fMLP stimulation in neutrophils.

2.2. fMLP internalization occurs rapidly in neutrophil

To further study endocytosis during neutrophil polarization, we next sought to characterize the kinetics of fMLP internalization. An early study quantified the endocytosis rate in polymorphonuclear leukocytes using fluorescein-dextran and observed a steady increase in intensity over time [14]. We used FITC-labeled fMLP to track internalization of fMLP over time using flow cytometry analysis. Similar to the canonical transferrin uptake assay to quantify the endocytic rate [13], we measured the intensity of FITC-fMLP following surface-bound ligand removal. Due to the incomplete differentiation of some cells, we observed two populations in the FITC channel (Sup Fig. 1). The peak intensities for two contiguous time points only had small differences. In this case, using a simple mean or median or any manually picked metrics would fail to quantify the data objectively. Hence, we resorted to a Gaussian mixture model to model the two populations by assuming that the data came from two Gaussian distributions and extracted the larger mean as the "average intensity" for that sample. The method has several advantages in this application: 1. it utilized all the acquired data without manually excluding any data; 2. it was able to differentiate the difference between conditions; 3. it was robust across all independent experiments.

We observed a canonical endocytic uptake trend for the uptake of fMLP within the first 20 minutes (Fig. 2A and B), similar to that of transferrin receptor (Sup Fig. 2A). It is worth noting that the rate of increase is not uniform in the first 20 min. The rate of increase between 0 min to 2 min was much more distinct than any other time range (1.43 ± 0.069 a.u./min), and followed by 5 min−10 min (0.0237 ± 0.0118 a.u./min). In contrast to previous reported results, we observed a drop in FITC-fMLP intensity at 30 min, following robust internalization at earlier time points. One possible reason is that ligands undergo complex endocytic pathways, along which the ligand-receptors get recycled back to the membrane or degraded within the cells.

2.3. CME is important for neutrophil polarization

The association of FPR with CCPs and internalization of fMLP bound FPR following fMLP stimulation suggest that CME might play a role in neutrophil

https://doi.org/10.1016/j.heliyon.2018.e00819

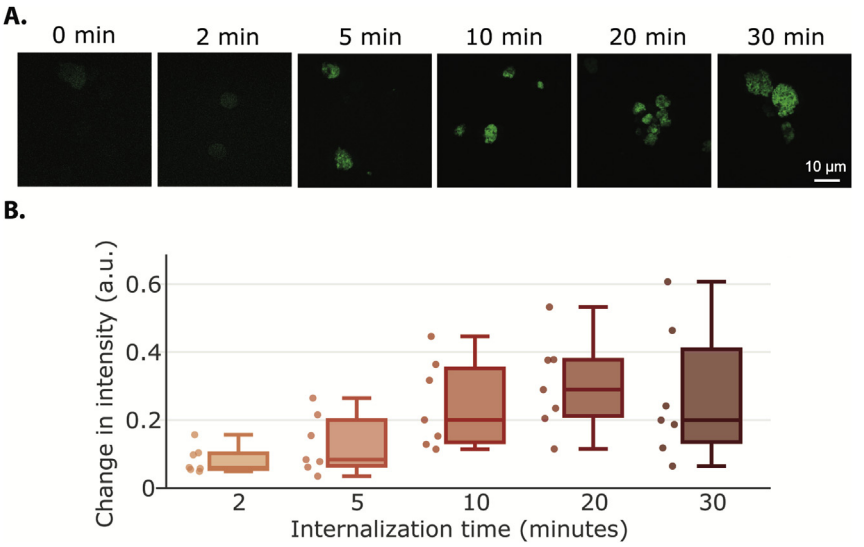

Fig. 2. fMLP internalization first increases over time but then decreases. (A) Differentiated neutrophils starved for 30 min were treated with 200 nM of FITC-fMLP and fMLP internalization at 0, 2 min, 5 min, 10 min, 20 min, and 30 min time points were imaged by confocal microscopy. (B) fMLP internalization at different time points were measured by flow cytometry (See Materials andMethods for detailed calculation of 'average intensity'). Each data point for a specific condition in the box plot represents the difference in average intensity between that condition and the control condition (without internalization) from a single experiment. A total of 7 independent experiments were performed.

polarization. To investigate whether CME is essential in neutrophil polarization, we resorted to pharmaceutical perturbations, which acutely and effectively target cell population and do not suffer from compensation in genetic knockdown experiments. We performed experiments with two of the mostly used inhibitors for CME, Pitstop2 (that interferes with CCP assembly [15]) and Dynasore (that inhibits vesicle scission [16]). Both of these inhibitors blocked fMLP-induced FPR endocytosis (Sup Fig. 2B and C). Due to the potential off-target effects of Pitstop2 that has been reported to block clathrin-independent endocytosis [17, 18], results obtained from using Pitstop2 are included in supplemental material. It is worth noting that there have also been non-specific effects reported for Dynasore [19, 20]. In order to evaluate the effects of endocytosis inhibitors on neutrophil polarization in an objective manner, we used automated imaging and analysis of fixed cells labeling microtubule, actin, phospho-myosin II (pMyosinII) and DAPI (Fig. 3A and B, Sup Fig. 3A). In fMLP-treated cells, actin and microtubule/pMyosinII distinctively localized to the front and rear of a cell, respectively. As it is readily apparent, addition of Pitstop2 and Dynasore abrogated fMLP-induced polarization.

To precisely quantify differences in polarization, we extracted three groups of features from the images: morphology (C1 and C2), center (C3-C5), and intensity (C6-C8) (Fig. 3E). To avoid possible selection bias, we analyzed about 1000 cells for each condition. Due to the large number of cells imaged, we need a more

https://doi.org/10.1016/j.heliyon.2018.e00819

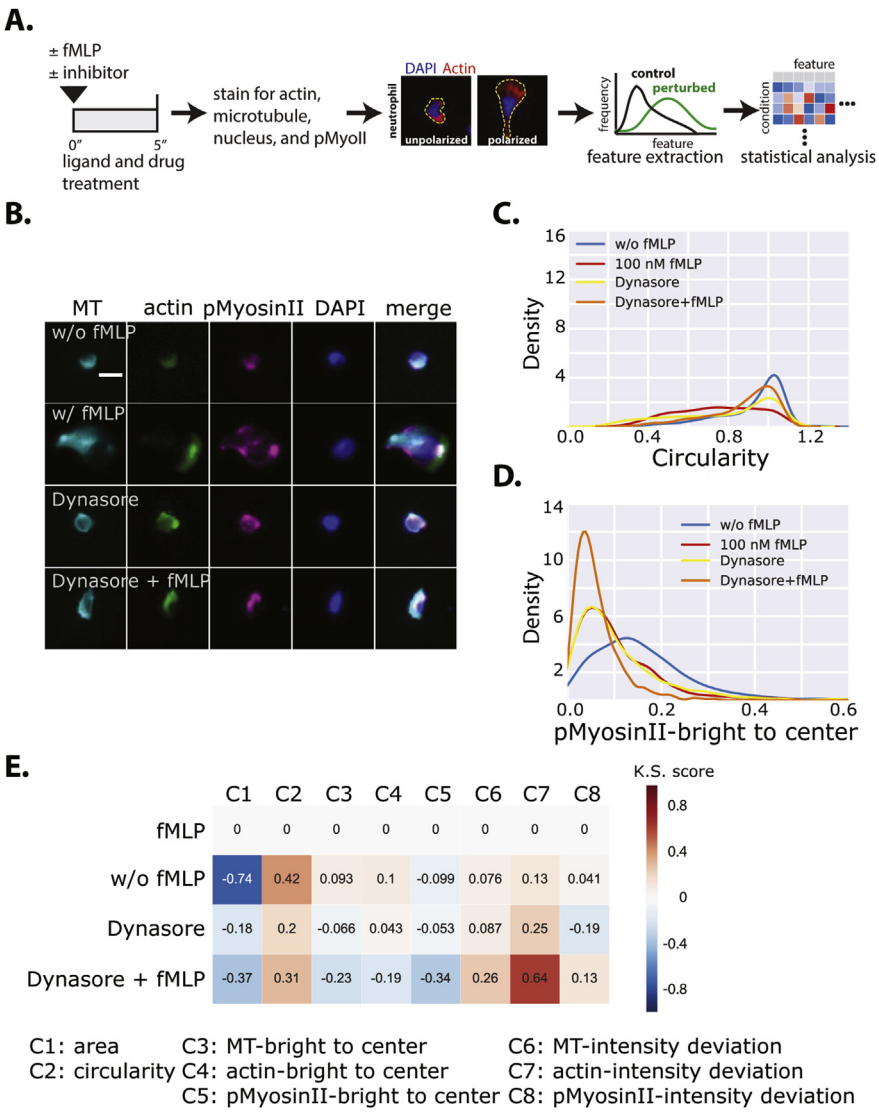

Fig. 3. Dynasore, a drug that perturbs clathrin-mediated endocytosis, inhibits neutrophil polarization. (A) Schematic of the experiment procedure. (B) Representative fluorescence images (cyan: microtubule, green: actin, magenta: pMyosinII, blue: DAPI) of neutrophils with and without fMLP and Dynasore. (C)−(D) Kernel density estimation for circularity and relative distance between bright spot of pMyosinII to cell center distributions in different conditions. Two example distributions from 18 extracted features are shown here. (E) Kolmogorov-Smirnov test statistics between the 100 nM fMLP condition and the rest of the conditions. A positive value indicates that the distribution for the feature shifts to the right compared to the fMLP condition (e.g., circularity distribution in Fig. 3C). A negative value indicates a shift to left (e.g., pMyosinII-bright to center in Fig. 3D). ($n_{w/o\ fMLP} = 1358$, $n_{fMLP} = 764$, $n_{Pitstop} = 1423$, $n_{Pitstop+fMLP} = 894$, $n_{Dynasore} = 1572$, $n_{Dynasore+fMLP} = 1421$.) An absolute value of K.S. score greater than 0.061 indicate significantly different distributions (see Materials andMethods).

compressed way to represent the feature for each condition. In high-throughput screening studies for selecting hits, *z*-score method, *B*-score method, strictly standardized mean difference, and quantile-based methods are used as a way to summarize thousands of measurements into a single number [21]. As illustrated in Fig. 3C

https://doi.org/10.1016/j.heliyon.2018.e00819

and D, the data were not drawn from a normal distribution; therefore, we adopted Kolmogorov-Smirnov (KS) test statistics to summarize distributions (more details can be found in Sup Fig. 4). Using the fMLP stimulation condition as the base, a negative KS score (in blue) would mean that the distribution of the measurement shifts to the left compared to fMLP-stimulated cells, and therefore is on average smaller. On the other hand, a positive KS score (in red) would mean that the distribution shifts to the right, and therefore is on average larger (Fig. 3E). For example, in the case of untreated neutrophils, KS score was negative for cell area but positive for circularity (circularity = 1 when it is a perfect circle) (Fig. 3E and Sup Fig. 3C). It is well known neutrophils are smaller and rounder compared to those stimulated with fMLP and our data provides an assuring proof-of-principle for our analysis. Using this analysis, we observed the same pattern for both Pitstop2 and Dynasore-treated neutrophils with and without fMLP. However, Dynasore-treated neutrophils had less negative KS statistics for cell area, indicating that Pitstop2 had a larger effect on morphological phenotype.

Besides morphological features, we further measured center and intensity features, denoted as 'bright to center' and 'intensity deviation', that characterized the spatial organization for microtubules, actin and pMyosinII (Fig. 3D). The center feature characterizes how polarized a structure is, and is calculated as the normalized distance (by the cell diameter) between the center of an area with 95% of total intensity pixels within a cell and the centroid of all the pixels within a cell. If the 95% brightest pixels all concentrate in a small region along the cell edge, then center feature is large. On the contrary, if the brightest pixels are close to the center or around the cell periphery, then the value would be small. For cells without fMLP, we only observed a marginal difference in center features compared to cells stimulated with fMLP (Fig. 3E). For Pitstop2 and Dynasore-treated fMLP stimulated cells, center features were on average smaller, suggesting that Pitstop2 and Dynasore impaired distribution of actin, microtubule, and pMyosinII (Fig. 3E and Sup Fig. 3C). Intensity deviation calculates the standard deviation in fluorescence intensity within a cell. A small value means a narrower distribution of the intensity, whereas a large value means intensities within a cell are more spread out. Interestingly, for microtubule and actin, our analysis indicated a larger standard deviation but a smaller bright to center distance for cells without fMLP and for cells treated with Pitstop2 or Dynasore with or without fMLP. From the fluorescence images, we could see a bright band of actin and microtubule at the end of a cell in Pitstop2 and Dynasore-treated cells, which explains the large variance, but the distance to the center is not as large compared to the cells treated with fMLP. It is worth pointing out that Dynasore has been shown to affect actin polymerization in a dynamin-independent mechanism [22, 23]. However, besides changes in actin assembly, we also found changes in microtubule and pMyosinII, which suggest that this could still be due to Dynasore's effect on endocytosis. Taken together, perturbation of

https://doi.org/10.1016/j.heliyon.2018.e00819

CME by Pitstop2 and Dynasore caused disruption of neutrophil polarization. Even though we cannot rule out off target effects of these small molecules on the cells [18, 19, 20, 24], the finding that both small molecule inhibitors targeting endocytosis abrogated neutrophil polarization suggest that CME plays a crucial role in neutrophil polarization.

2.4. Inhibition of CME blocks several signaling pathways

Many studies have pointed to the crucial and multi-faceted roles of CME on signaling [12, 25, 26, 27, 28]. Clathrin's role as a scaffold but not in receptor endocytosis is required for Akt_{308} phosphorylation upon epidermal growth factor stimulation [12, 27]. In an analogous way, Eichel et al. revealed that clathrin-coated structures on the plasma membrane are central for β-arrestin signaling of GPCRs [29]. Conversely, proper CME is important for other signaling pathways, including ERK and mTORC1 signaling [12]. The importance of endocytosis for downstream signaling has also been found in growth factor signaling to mTORC1 in macrophages [30]. Since Pitstop2 and Dynasore both potently blocked fMLP-induced neutrophil polarization, we hypothesize that these inhibitors also block cell signaling. To investigate the downstream signaling effectors of CME, we compared $pAkt_{308}$, $pAkt_{473}$ and pERK levels without and with Pitstop/Dynasore in fMLP stimulated cells. $pAkt_{308}$, $pAkt_{473}$ and pERK covered three major signaling pathways. Specifically, $pAkt_{308}$ indicates the activities of protein kinase Akt, which mediates the positive feedback loop between PIP_3 and actin [31], $pAkt_{473}$ was used as a readout of PIP_3 and mTORC2 activity, and pERK is activated in the MAPK/ERK pathway that is frequently associated with the β-arrestin signaling pathway. Using Western blot analysis, we measured the phosphorylation of $pAkt_{308}$ (Fig. 4A and B, Sup Fig. 5A and B), $pAkt_{473}$ (Fig. 4C and D, Sup Fig. 5C and D), and pERK (Fig. 4E and F, Sup Fig. 5E and F) at various time points between 0 min to 10 min and observed a rapid stimulation which reached its peak within 1−2 minutes and gradually decreases. However, all these dynamical changes disappeared when cells were treated with Pitstop2 (Sup Fig. 5). Pitstop2 blocks CME at the early stage but not the binding of fMLP to FPR. Hence, we could speculate that proper assembly of CCPs is a crucial step in effective signal transduction. It is interesting to note that Dynasore's impact on neutrophil polarization was not as dramatic as that of Pitstop2 (Fig. 3E and Sup Fig. 3C). Here, our signaling analysis showed that the peak intensities of $pAkt_{308}$, $pAkt_{473}$, and pERK of cells in the presence of Dynasore were about half compared to untreated cells, which might explain the intermediate phenotype of Dynasore-treated cells. Even though Dynasore-treated cells also reached maximum signaling between 1 and 2 minutes, the subsequent decline of signaling was less efficient. From these results and those in the previous section, we believe that CME inhibition hindered neutrophil polarization by blocking fMLP-induced signaling.

https://doi.org/10.1016/j.heliyon.2018.e00819

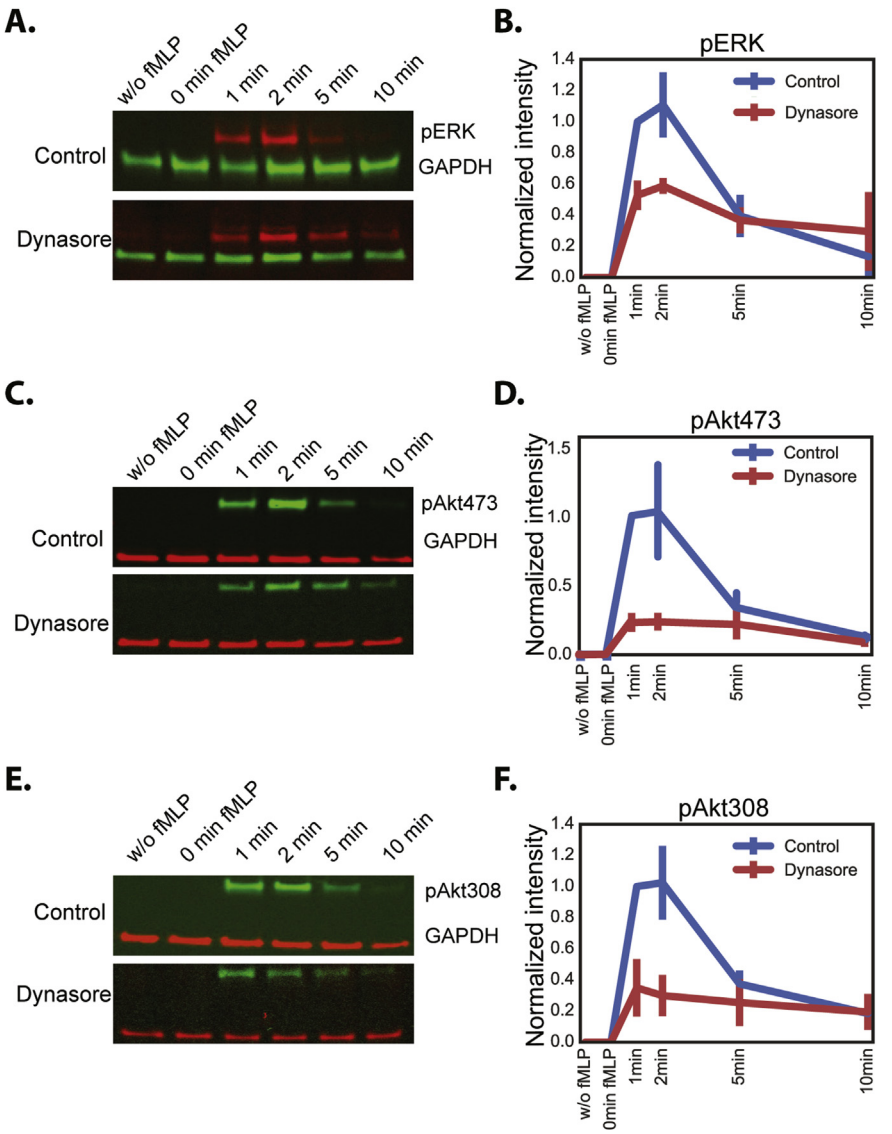

Fig. 4. Inhibition of CME blocks several signaling pathways. Changes of pERK (A, B) $pAkt_{473}$ (C, D), and $pAkt_{308}$ (E, F) were quantified from analysis of cropped Western blots in samples with and without fMLP over time with and without Dynasore. Data in B, D, and F represented mean ± s.e.m. from three independent experiments. Full Western blots are shown in Sup Fig. 6.

2.5. Polarized neutrophils have denser and dimmer CCPs at the front

The differences between fMLP stimulation and the two small molecule inhibition conditions provide some clues on the role of CME during neutrophil polarization. Signal transduction likely occurs concurrently during CCP formation, invagination, and scission to form clathrin-coated vesicles (CCVs). More importantly, the events after CCP scission (where max signaling is 1−2 minutes) may also aid in neutrophil polarization (on the order of 5 minutes). To gain deeper insights on the relationship

https://doi.org/10.1016/j.heliyon.2018.e00819

of clathrin machinery and signaling scaffold with neutrophil polarization, we investigated in detail the spatial organization between actin, the prominent structure that marks polarity, and clathrin or β-arrestin, the structural and signaling scaffolds in CME, respectively.

As shown in Fig. 3, neutrophil polarization is marked by the non-uniform cellular components, such as actin, microtubule, and pMyosinII. However, there have been a number of inconsistent reports on the spatial distribution of CCPs in polarized cells. In 1982, Davis *et al.* observed that CCPs were mainly located at the back of polarized neutrophils *via* transmission electron microscopy [8]. However, Rappoport and Simon reported that the majority of CCPs were at the leading edge of a migrating cell [9]. We believe that these incongruent findings may lie in the methods used to observed CCP. From our own experiments, CCPs appear to preferentially localize at the front end of the cells by TIR-FM where the ventral plasma membrane is visualized. On the other hand, CCPs appear to be in the middle or at the back of the cell when using confocal or epi-fluorescence microscopy [6, 32]. Here we use TIR-FM for better signal-to-background ratio and more accurate CCP localization.

Consistent with previous studies, we also observed polarization in CCP localization. Without fMLP, CCPs were more evenly distributed on the membrane, whereas there was a distinct CCP band well correlated with the lamellipodia in polarized cells (Fig. 5A). As we and others have shown [33], fMLP stimulation leads to rapid polymerization of actin filaments, as evidenced by an increase in phalloidin-stained actin intensity (Fig. 5B and C). We observed the same trend for CCPs (Fig. 5D and E). There were about 5 times more CCPs and a right shift of intensity distribution in fMLP-stimulated cells, with a slightly higher density. In Fig. 1D and E, we noted that there appeared to be more dimmer CCPs in the presence of fMLP. Here, we indeed observed the CCP intensity distribution was left-skewed with a long tail. However, compared to the cells without fMLP, the CCP median intensity was still higher.

With more and brighter CCPs in the presence of fMLP, how were they distributed on the cell membrane? From the microscopy images, we observed that near the bright actin staining, CCPs also seemed to be denser. To quantify this observation, we calculated the local CCP density and actin intensity for each CCP by drawing a circle centered at it. For actin intensity, we chose a small radius of 5 pixels ($\sim$290 nm) to reflect local density. For CCP density, we selected a larger radius of 40 pixels ($\sim$2.33 μm) to capture its spatial organization. We also calculated the average intensity for all the CCPs within the circle. Therefore, for each point in Fig. 5F and G, it represents an individual CCP and shows its local CCP density, actin intensity, and the average CCP intensity (indicated by the size of the point). Comparing the cells without fMLP (Fig. 5F) and with fMLP (Fig. 5G), we saw a striking difference in CCP distribution and their correlation to actin intensity. Without fMLP, there

https://doi.org/10.1016/j.heliyon.2018.e00819

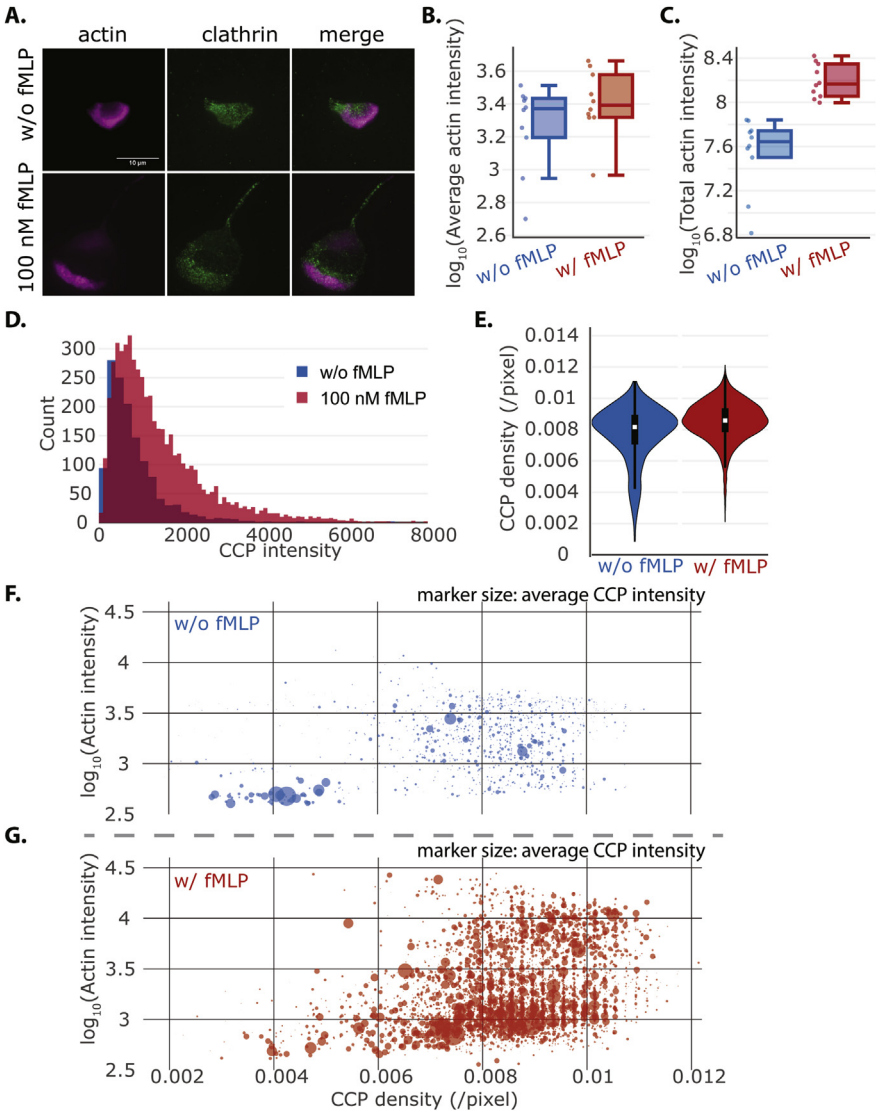

Fig. 5. There is a dramatic increase in CCP numbers and intensity in the presence fMLP. (A) Representative TIRF images of actin (magenta) and CCPs (green) without (upper) and with (bottom) 100 nM fMLP. (B)−(C) Boxplot of average actin intensity and total actin intensity across the whole cell. Each dot represents an individual cell. $p^* = 0.29$, Wilcoxon rank-sum test for average actin intensity. $p^{**} = 0.00015$, Wilcoxon rank-sum test for total actin intensity. ($n_{w/o\ fMLP} = 10$, $n_{100\ nM\ fMLP} = 10$) (D) Histogram of CCP intensities with and without fMLP. The data were from the same cells as the ones in which actin intensities were measured. $p \sim 0$, Kolmogorov-Smirnov test. ($n_{w/o\ fMLP} = 1361$, $n_{100\ nM\ fMLP} = 5364$) (E) Violin plot of CCP densities with and without fMLP. $p < 10^{-26}$, Kolmogorov-Smirnov test. (F)−(G) Scatter plot of CCP density *vs.* local actin intensity (in log scale). Each dot in the plot denotes an individual CCP with *x*-axis representing CCP density and *y*-axis is the local actin intensity. The size of the dot represents the average CCP intensity. CCP density in a radius of 40 pixels and local actin intensity radius of 5 pixels were used in this analysis.

https://doi.org/10.1016/j.heliyon.2018.e00819

were two distinct populations of CCPs, a larger one with low actin intensity and low CCP density and a second population with higher actin intensity and larger CCP density. This separation completely disappeared with fMLP stimulation. However, we observed that most CCPs resided at the lower triangle of the plane, which means that when actin intensity was low, CCP density was not constrained. At high actin intensity areas, CCP density scaled up as well. Interestingly, at the top right part of the plane, where actin intensities and CCP densities were both high, CCP intensities on average were dimmer. This result is consistent with our finding in Fig. 1 where dimmer CCPs had more FPRs. The result also agrees with our recent finding that small and short-lived CCPs are capable of signaling [12]. Together, our analysis provides clear evidence that fMLP stimulation promotes nucleation of CCP and suggests the endocytic machineries signal to actin polymerization in neutrophil polarization. The observation of smaller CCPs is consistent with previous findings that cells with high tension have smaller CCPs [34, 35] where we expect the leading edge of the cell to have higher membrane tension [36]. Previous work has demonstrated that receptor clustering can promote CCP nucleation [13]. Ligand binding and receptor clustering is a cellular mechanism to control receptor signaling [37], so it is plausible that the dim CCPs represent *de novo* nucleated CCPs upon FPR clustering.

2.6. There is a dramatic increase in the number and intensity of β-arrestin in polarized neutrophils

We speculate the endocytic machineries have to signal to actin assembly during neutrophil polarization so there should be a spatial relationship between signaling scaffold proteins and actin structures. Our signaling experiments showed CME played an important role in ERK phosphorylation and it has been shown that pERK reinforces actin polymerization at the leading edge during motility [38]. G protein-independent ERK activation has been shown to be dependent on β-arrestin [39]. Recent work has also shown that FPR signaling is mediated by β-arrestin [2], and we observed colocalization of FPR and β-arrestin when neutrophils are stimulated with fMLP (Sup Fig. 7). Based on these reasons, we investigated the spatial relationship between β-arrestin, acting as a scaffold intermediates for GPCR signaling, and actin structures.

We observed a more distinct difference in β-arrestin immunofluorescence between fMLP stimulation and no stimulation compared to clathrin. Without fMLP, β-arrestin only formed dim punctate structures, but in the presence of fMLP, punctate structures were much more discernible and distributed all over the cell membrane (Fig. 6A). The β-arrestin structures were not only brighter, but the distribution also appeared denser. Following the same analysis as described earlier,

https://doi.org/10.1016/j.heliyon.2018.e00819

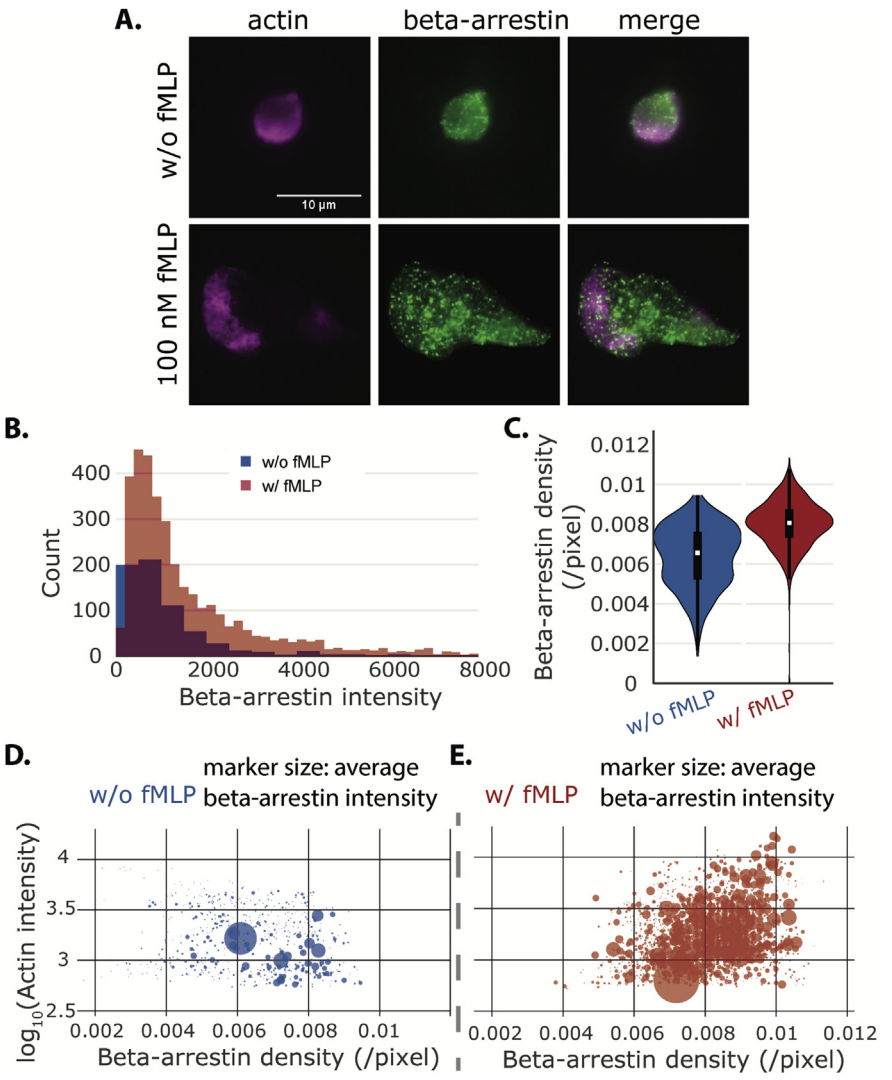

Fig. 6. fMLP greatly increases the number of β-arrestin on the membrane. (A) Representative TIRF images of actin (magenta) and β-arrestin (green) without (upper) and with (bottom) 100 nM fMLP. (B) Histogram of β-arrestin intensities with and without fMLP. $p < 10^{-11}$, Kolmogorov-Smirnov test. (Cell number: $n_{w/o\ fMLP} = 8$, $n_{100\ nM\ fMLP} = 10$; β-arrestin number: $n_{w/o\ fMLP} = 659$, $n_{100\ nM\ fMLP} = 3540$) (C) Violin plot of β-arrestin densities with and without fMLP. $p \approx 0$, Kolmogorov-Smirnov test. (D)−(E) Scatter plot of β-arrestin density *vs.* local actin intensity (in log scale). Each dot in the plot denotes an individual β-arrestin with *x*-axis representing β-arrestin density and *y*-axis the local actin intensity. The size of the dot represents the average β-arrestin intensity. β-arrestin density based on radius of 40 pixels and local actin intensity radius of 5 pixels were used in this analysis.

the β-arrestin intensity histogram and density distribution were in agreement with this observation (Fig. 6B and C).

To better quantify the spatial organization of β-arrestin, we mapped each detected β-arrestin to local actin intensity and β-arrestin density space, with the marker size representing the β-arrestin intensity (Fig. 6D and E). The plot revealed a different

https://doi.org/10.1016/j.heliyon.2018.e00819

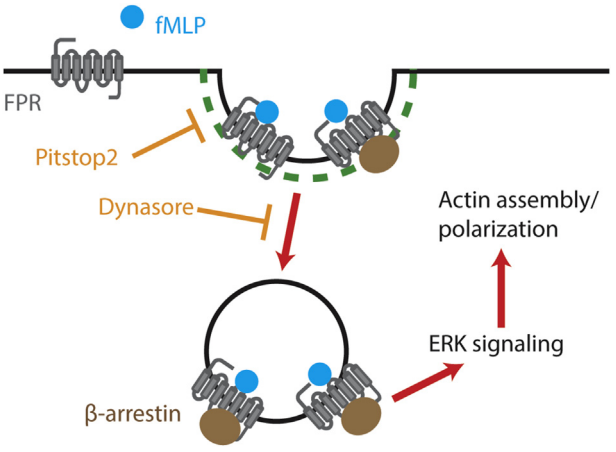

Fig. 7. Model summarizing the role of CME of fMLP receptor in mediating neutrophil polarization. Spatially localized internalization of fMLP receptor is important for signaling to the actin cytoskeleton during neutrophil polarization.

pattern for β-arrestin than clathrin. Like clathrin distribution, we find high β-arrestin density at high actin intensity, although there is a range of β-arrestin density. However, at regions with high actin intensity with fMLP stimulation (*i.e.* top right corner of the plot), we found more and brighter β-arrestin structures (recall clathrin was dimmer in this region). The difference between clathrin and β-arrestin distribution may reflect the functional and temporal disparities of the two molecules. Clathrin recycles between polymerization and uncoating during the formation of CCVs whereas β-arrestin needs to sustain signaling to actin polymerization during polarization and motility.

3. Conclusion

By applying quantitative approaches, our studies have revealed a tight connection between endocytosis of FPR receptor, signaling of fMLP-FPR, and functional polarization of neutrophils (Fig. 7). Assembly of CCPs and internalization of CCVs are critical for cell signaling and we believe that the ability to spatially organize a variety of molecules into its functional unit is one reason that CME is important in many physiological processes [40]. As discrete macromolecular assemblies, CCPs can spatially organize cell signaling with spatiotemporal precision. A theoretical study has predicted that polarity requires optimal endocytosis and can be dynamically stabilized through positive feedback with directed transport [41]. In this regard, cell polarization has been described as a bistable process with competition for actin between myosin II-dependent contractility and dendritic actin polymerization [42] that allows for retrograde transport of myosin II. Our work shows the critical role CME plays in signaling to actin polymerization, without which polarization would be blocked. As receptor clustering and CCP initiation can be tuned depending on

https://doi.org/10.1016/j.heliyon.2018.e00819

chemical and mechanical microenvironment, a cell would be able to rapidly make migration decisions during chemotaxis by integrating information from CCPs.

4. Materials and method

4.1. Cell culture and differentiation

We received HL-60 cell as a gift from Dr. Orion Weiner (UCSF). HL-60 cells were maintained in RPMI medium supplemented with 10% heat-inactivated FBS and 1% penicillin streptomycin at 37 °C/5% CO_2. Neutrophil-like cells used in experiments were differentiated from HL-60 by introducing 1.5% DMSO into growth medium for 3−6 days.

4.2. Flow cytometric analysis of fMLP or transferrin internalization

The flow cytometry assay was performed to measure the internalization of fMLP. Differentiated cells were first serum-starved for 30 min at 37 °C and then incubated with 100 nM fluorescein conjugate of formyl-Nle-Leu-Phe-Nle-Tyr-Lys (abbreviated as FITC-fMLP) (F1314, Thermo Fisher Scientific, MA) or 25 μg/ml of Alexa Fluor 647 conjugated transferrin (T23366, Thermo Fisher Scientific, MA) on ice for 30 min to equilibrate the binding between ligands and receptors. The cells were transferred to 37 °C water bath and incubated for the indicated amount of time, while keeping one sample on ice as a control. The endocytosis was halted by adding a volume of ice-cold mHBSS and returning the sample to ice. Samples were then spun at 400× g to pellet and washed with acid buffer (500 mM Glycine in mHBSS, pH = 2.7) to remove surface bound ligand molecules, followed by two more ice-cold mHBSS washes. The samples were measured within an hour using Guava easyCyte flow cytometer (Millipore, MA).

4.3. Fibronectin coverslip coating

In order for cells to adhere to the surface, all coverslips were coated with 100 μg/mL fibronectin (F4759, Sigma, MO) in Ca^{2+}/Mg^{2+}-free PBS for 1 hr. The coated coverslips were then washed twice with Ca^{2+}/Mg^{2+}-free PBS and incubated in mHBSS with 1% endotoxin-free human serum albumin (Gemini Bio-Products, CA) for more than 15 min. They were used within the day of preparation.

4.4. Immunostaining

For immunostaining, cells were fixed in ice-cold 3.7% paraformaldehyde in intracellular buffer (140 mM KCl, 1 mM $MgCl_2$, 2 mM EGTA, 320 mM sucrose, and 20

https://doi.org/10.1016/j.heliyon.2018.e00819

mM HEPES with pH 7.5) for 45 min on ice. For imaging fMLP internalization, cells were washed with acid buffer (500 mM Glycine in mHBSS, pH = 2.7) prior to fixation. After washing and permeabilization with 1% Triton X-100, cells were then blocked in intracellular buffer containing 1% bovine serum albumin for 1 hr, before incubating with primary antibody overnight at 4 °C. On the second day, after washed six times with PBS, samples were incubated with secondary antibody along with rhodamine-phalloidin (PHDR1, Cytoskeleton, CO) and DAPI (D9542, Sigma-Aldrich, MO) for 3 hours at room temperature at manufacturer's recommended concentrations. Cells were imaged after washing with PBS.

In immunostaining experiments, we have used the following antibodies: AF647 mouse − α-human fMLP receptor (565623, BD Biosciences, CA), phospho-myosin light chain2 (Ser19) antibody (#3675, Cell Signaling Technology, MA), α-tubulin antibody (#2144, Cell Signaling Technology, MA), clathrin antibody [X22] (ab2731, Abcam, MA), β-arrestin-1/2 antibody (sc-74591, Santa Cruz Biotechnology, TX).

4.5. Spatial correlation between CCP and FPR

CCPs and FPRs were imaged using TIR-FM. CME Analysis software was used to detect the location and intensity of each CCP and FPR. Next, to quantify the spatial correlation between two structures, we calculated the following quantities for each CCP. Without loss of generality, consider CCP_i with center location (x_c, y_c):

1. The number of FPRs within 10-pixel radius of CCP_i:

$$num\ \ of\ FPR|_{CCP_i} = \sum_{(x_j,y_j)\in detected\ FPR} \mathbb{L}\left(R_d^2 - \left(\left|x_j - x_i\right|^2 + \left|y_j - y_i\right|^2\right)\right)$$

where $\mathbb{L}(x) = \begin{cases} 1 & x \geq 0 \\ 0 & x < 0 \end{cases}$, $R_d = 10$ pixel.

2. The average intensity of all the FPRs within 10-pixel radius of CCP_i:

$$average\,intensity\,of\,FPR|_{CCP_i} = \frac{\sum_{(x_j,y_j)\in detected\,FPR} A_j^{FPR}\mathbb{L}\left(R_d^2 - \left(\left|x_j - x_i\right|^2 + \left|y_j - y_i\right|^2\right)\right)}{\sum_{(x_j,y_j)\in detected\,FPR}\mathbb{L}\left(R_d^2 - \left(\left|x_j - x_i\right|^2 + \left|y_j - y_i\right|^2\right)\right)}$$

where A_j^{FPR} is the intensity of FPR detected at (x_j, y_j).

Each individual CCP is mapped to a plane where x-axis is the CCP intensity and y-axis the number of FPR puncta surrounding it (the first quantity above) with the marker size indicating the average FPR intensity (the second quantity).

https://doi.org/10.1016/j.heliyon.2018.e00819

4.6. Microscopy for fixed samples

We employed different imaging systems for different experiments. To observe clathrin and β-arrestin, we used total internal reflection fluorescence microscopy; for each cell, we also recorded the actin and nucleus using epi-fluorescence microscopy which is available on the same microscope. TIR-FM was performed on a Nikon TiE-Perfect Focus System (PFS) microscope equipped with an apochromat 100X objective (NA 1.49), a sCMOS camera (Flash 4.0, Hamamatsu Photonics, Japan), and a laser launch controlled by an acoustooptic tunable filter (AOTF).

To measure the effect of drug treatments on neutrophil polarization, cells were stained with α-tubulin, phospho-myosin light chain 2, actin and nucleus and imaged using Cytation 5 Cell Imaging Multi-Mode Reader (BioTek, VT) equipped with 20X objective and DAPI, GFP, RFP, and Cy7 imaging filter cubes.

4.7. Kolmogorov-Smirnov (KS) test

KS test was used to test if the two one-dimensional probability distributions differ. The null-hypothesis between two distributions is rejected at α at:

$$D_{n,m} > c(\alpha)\sqrt{\frac{m+n}{mn}}$$

where n and m are the sizes of the first and second distribution, c is a threshold that depends on the level of significance α, $D_{n,m}$ is the absolute value of the KS test.

In our studies, $m,n \approx 1000$, if we want to reject the null-hypothesis at level $\alpha = 0.05$, which means $c(\alpha) = 1.36$, then we will have $D_{1000,1000} > 1.36 \times \sqrt{\frac{1}{500}} = 0.061$.

4.8. Spatial correlation between CCP/β-arrestin and actin

CCP and β-arrestin structures were imaged using TIR-FM to obtain high-resolution and high signal-noise ratio pictures. CME analysis package was used to faithfully detect the dot-like structures (for CCPs and β-arrestin) [11]. For each dot-like structure, its location $(x_i,\ y_i)$ and intensity A_i in the cell was determined. To obtain the correlation between CCP/β-arrestin and actin intensity, we calculated the local density for each detected CCP/β-arrestin as well as the corresponding intensity at the same location for actin. The density can be formulated mathematically:

$$\text{local density}|_{(x_j,y_j)} = \frac{\sum_{(x_i,y_i)\in \text{detected pucta}} \mathbb{L}\left(R_d^2 - \left(|x_i - x_j|^2 + |y_i - y_j|^2\right)\right)}{\pi R_d^2}$$

where $\mathbb{L}(x) = \begin{cases} 1, & x \geq 0 \\ 0, & x < 0 \end{cases}$, R_d is the radius we used to calculated the local density for dot-like structures, and (x_i, y_i) is the coordinates we obtained from the detection results. Similarly, local actin intensity can be formulated:

https://doi.org/10.1016/j.heliyon.2018.e00819

$$\text{local actin intensity}|_{(x_i,y_i)} = \frac{\sum_{\substack{a\in[x_i-r,\ x_i+r]\\ b\in[y_i-r,\ y_i+r]}} \text{ActinImage}(a,b)}{\pi r^2}$$

where $\text{ActinImage}(a,b)$ is the intensity at (a,b) for actin image, r is the radius within which we counted the pixel as local. We selected different values for R_d and r: we wanted to count a reasonable number of CCP/β-arrestin structures but they were somewhat sparse, but for actin intensity we could choose a relatively small radius so that we could average the potential noise yet still have a good approximation at a specific location.

4.9. Polarization quantification

In order to unbiasedly quantify drug effect on neutrophil polarization, we used Cytation 5 imager to take around 1000 cells per condition. A customized CellProfiler pipeline, which implemented watershed algorithm, was applied to the images to effectively generate the masks for individual cells. To overcome over-segmentation of the watershed algorithm, we used DAPI as the marker image, added up three other channel images (MT, actin and pMyosinII) as the secondary image, and then applied the watershed algorithm. We then manually inspected every cell/mask pair and discarded the cells which were mistakenly segmented. Using the generated masks, we calculated the following morphological features: area, perimeter, circularity, solidity, eccentricity, major axis length, minor axis length and equivalent diameter. Employing both the staining image and mask, we quantified the intensity features and center features, which are listed in Sup Table 1. The feature extraction was implemented in MatLab.

4.10. Western blot analysis

For Western blots, an equal volume of ice-cold 20% trichloroacetic acid (TCA) was added to the sample to lyse the cells. 40 mM NaF and 20 mM β-glycerophosphate were included if blotting against the phospho-proteins. The mixtures were then kept at 4 °C overnight for maximum yield of proteins. Lysates were then centrifuged at 13,000×g at 4 °C for 5 min to pellet. The pellets were then washed in 0.5% TCA once and then resuspended in 50 μL 2× Laemmli sample buffer (1610737, Bio-Rad, CA) containing 30 mM NaOH and 5% β-mercaptoethanol. Protein bands were separated by SDS-PAGE gel electrophoresis and transferred to nitrocellulose membrane. The membrane was blocked with 5% milk and incubated overnight with following antibodies: CHC [TD.1] (24578, Abcam, MA); pAkt308 (2965 or 4056, Cell Signaling Technology, MA); pAkt473 (4060, Cell Signaling Technology, MA); total Akt (4691, Cell Signaling Technology, MA); pERK (9106 or 4376, Cell Signaling Technology, MA); GAPDH (24778, Santa Cruz Biotechnology, TX); actin (8432, Santa Cruz Biotechnology, TX). The blots were developed with fluorescent secondary antibodies: goat anti-mouse DyLight 680 (35518, Thermo Fisher

https://doi.org/10.1016/j.heliyon.2018.e00819

Scientific, MA) and goat anti-rabbit DyLight 800 (SA5-10036, Thermo Fisher Scientific, MA), and the blots were imaged using Odyssey Infrared Imaging System (Li-COR, Biosciences, NE) under the same setting. The Western blot results were quantified using ImageJ. At least three independent experiments were conducted for each condition.

4.11. Drug treatment

For Pitstop2 and Dynasore experiments, cells were first serum-starved for 30 min and then pre-incubated with 25 μM Pitstop2 (ab120687, Abcam, MA) or 75 μM Dynasore (ab120192, Abcam, MA) for 15 min; then experimental groups were stimulated with 100 nM fMLP for 5 min at 37 °C, during which control groups were kept in 37 °C, before halting the stimulation by adding a volume of ice-cold 2x fixation buffer (7.4% paraformaldehyde in 2x intracellular buffer).

Declarations

Author contribution statement

Xinyu Tan: Conceived and designed the experiments; Performed the experiments; Analyzed and interpreted the data; Contributed reagents, materials, analysis tools or data; Wrote the paper.

Mingzhi Luo: Performed the experiments; Analyzed and interpreted the data.

Allen P. Liu: Conceived and designed the experiments; Analyzed and interpreted the data; Wrote the paper.

Funding statement

Mingzhi Luo acknowledges support from the Key Program of NSF of China (No. 11532003) and Jiangsu Oversea Visiting Scholar Program for University Prominent Young and Middle-aged Teachers and Presidents. Allen P. Liu is supported by NSF-BMMB 1561794. Xinyu Tan was supported by Helen Wu Award and Rackham Summer Award.

Competing interest statement

The authors declare no conflict of interest.

Additional information

Supplementary content related to this article has been published online at https://doi.org/10.1016/j.heliyon.2018.e00819.

Acknowledgements

We thank Tejeshwar Rao and Arun Anantharam with help on HL-60 electroporation.

References

[1] A. Bagorda, C.A. Parent, Eukaryotic chemotaxis at a glance, J. Cell Sci. 121 (2008) 2621−2624.

[2] B.M. Wagener, N.A. Marjon, E.R. Prossnitz, Regulation of N-formyl peptide receptor signaling and trafficking by Arrestin-Src kinase interaction, PLoS One 11 (2016), e0147442.

[3] S. Ernst, N. Zobiack, K. Boecker, V. Gerke, U. Rescher, Agonist-induced trafficking of the low-affinity formyl peptide receptor FPRL1, Cell. Mol. Life Sci. 61 (2004) 1684−1692.

[4] F. Jean-Alphonse, A.C. Hanyaloglu, Regulation of GPCR signal networks via membrane trafficking, Mol. Cell. Endocrinol. 331 (2011) 205−214.

[5] A. Sorkin, M. Von Zastrow, Signal transduction and endocytosis: close encounters of many kinds, Nat. Rev. Mol. Cell Biol. 3 (2002) 600−614.

[6] B.L. Wolfe, J. Trejo, Clathrin-dependent mechanisms of G protein-coupled receptor endocytosis, Traffic 8 (2007) 462−470.

[7] M. Jose, S. Tollis, D. Nair, J.B. Sibarita, D. McCusker, Robust polarity establishment occurs via an endocytosis-based cortical corralling mechanism, J. Cell Biol. 200 (2013) 407−418.

[8] B.H. Davis, R.J. Walter, C.B. Pearson, E.L. Becker, J.M. Oliver, Membrane-activity and topography of F-Met-Leu-Phe treated polymorphonuclear leukocytes − acute and sustained responses to chemotactic peptide, Am. J. Pathol. 108 (1982) 206−216.

[9] J.Z. Rappoport, S.M. Simon, Real-time analysis of clathrin-mediated endocytosis during cell migration, J. Cell Sci. 116 (2003) 847−855.

[10] C. Kural, et al., Asymmetric formation of coated pits on dorsal and ventral surfaces at the leading edges of motile cells and on protrusions of immobile cells, Mol. Biol. Cell 26 (2015) 2044−2053.

[11] F. Aguet, C.N. Antonescu, M. Mettlen, S.L. Schmid, G. Danuser, Advances in analysis of low signal-to-noise images link dynamin and AP2 to the functions of an endocytic checkpoint, Dev. Cell 26 (2013) 279−291.

[12] L.K. Rosselli-Murai, et al., Loss of PTEN promotes formation of signaling-capable clathrin-coated pits, J. Cell Sci. 131 (2018).

https://doi.org/10.1016/j.heliyon.2018.e00819

[13] A.P. Liu, F. Aguet, G. Danuser, S.L. Schmid, Local clustering of transferrin receptors promotes clathrin-coated pit initiation, J. Cell Biol. 191 (2010) 1381−1393.

[14] B.H. Davis, E. McCabe, M. Langweiler, Characterization of f-Met-Leu-Phe-stimulated fluid pinocytosis in human polymorphonuclear leukocytes by flow cytometry, Cytometry 7 (1986) 251−262.

[15] L. von Kleist, et al., Role of the clathrin terminal domain in regulating coated pit dynamics revealed by small molecule inhibition, Cell 146 (2011) 471−484.

[16] E. Macia, et al., Dynasore, a cell-permeable inhibitor of dynamin, Dev. Cell 10 (2006) 839−850.

[17] D. Dutta, C.D. Williamson, N.B. Cole, J.G. Donaldson, Pitstop 2 is a potent inhibitor of clathrin-independent endocytosis, PLoS One 7 (2012), e45799.

[18] A.K. Willox, Y.M. Sahraoui, S.J. Royle, Non-specificity of Pitstop 2 in clathrin-mediated endocytosis, Biol. Open 3 (2014) 326−331.

[19] D. Basagiannis, S. Zografou, K. Galanopoulou, S. Christoforidis, Dynasore impairs VEGFR2 signalling in an endocytosis-independent manner, Sci. Rep. 7 (2017) 45035.

[20] G. Preta, J.G. Cronin, I.M. Sheldon, Dynasore − not just a dynamin inhibitor, Cell Commun. Signal. 13 (2015) 24.

[21] A. Birmingham, et al., Statistical methods for analysis of high-throughput RNA interference screens, Nat. Methods 6 (2009) 569−575.

[22] Q.C. Wang, et al., The Dynamin 2 inhibitor Dynasore affects the actin filament distribution during mouse early embryo development, J. Reprod. Dev. 61 (2015) 49−53.

[23] H. Yamada, et al., Dynasore, a dynamin inhibitor, suppresses lamellipodia formation and cancer cell invasion by destabilizing actin filaments, Biochem. Biophys. Res. Commun. 390 (2009) 1142−1148.

[24] E. Girard, et al., The dynamin chemical inhibitor dynasore impairs cholesterol trafficking and sterol-sensitive genes transcription in human HeLa cells and macrophages, PLoS One 6 (2011), e29042.

[25] A.P. Liu, R.J. Botelho, C.N. Antonescu, The big and intricate dreams of little organelles: embracing complexity in the study of membrane traffic, Traffic 18 (2017) 567−579.

[26] C.R. Reis, et al., Crosstalk between Akt/GSK3beta signaling and dynamin-1 regulates clathrin-mediated endocytosis, EMBO J. 34 (2015) 2132−2146.

https://doi.org/10.1016/j.heliyon.2018.e00819

[27] C. Garay, et al., Epidermal growth factor-stimulated Akt phosphorylation requires clathrin or ErbB2 but not receptor endocytosis, Mol. Biol. Cell 26 (2015) 3504−3519.

[28] Z.Y. Weinberg, A.S. Zajac, T. Phan, D.J. Shiwarski, M.A. Puthenveedu, Sequence-specific regulation of endocytic lifetimes modulates arrestin-mediated signaling at the micro opioid receptor, Mol. Pharmacol. 91 (2017) 416−427.

[29] K. Eichel, D. Jullie, M. von Zastrow, beta-Arrestin drives MAP kinase signalling from clathrin-coated structures after GPCR dissociation, Nat. Cell Biol. 18 (2016) 303−310.

[30] S. Yoshida, R. Pacitto, Y. Yao, K. Inoki, J.A. Swanson, Growth factor signaling to mTORC1 by amino acid-laden macropinosomes, J. Cell Biol. 211 (2015) 159−172.

[31] O.D. Weiner, et al., A PtdlnsP3-and Rho GTPase-mediated positive feedback loop regulates neutrophil polarity, Nat. Cell Biol. 4 (2002) 509.

[32] R. Samaniego, L. Sánchez-Martín, A. Estecha, P. Sánchez-Mateos, Rho/ROCK and myosin II control the polarized distribution of endocytic clathrin structures at the uropod of moving T lymphocytes, J. Cell Sci. 120 (2007) 3534−3543.

[33] C.-J. Ku, Y. Wang, O. Weiner, S.J. Altschuler, L.F. Wu, Evolving cross-talk in the neutrophil polarity network, Cell 149 (2012) 1073.

[34] E. Irajizad, N. Walani, S.L. Veatch, A.P. Liu, A. Agrawal, Clathrin polymerization exhibits high mechano-geometric sensitivity, Soft Matter 13 (2017) 1455−1462.

[35] X. Tan, J. Heureaux, A.P. Liu, Cell spreading area regulates clathrin-coated pit dynamics on micropatterned substrate, Integr. Biol. 7 (2015) 1033−1043.

[36] A.D. Lieber, Y. Schweitzer, M.M. Kozlov, K. Keren, Front-to-rear membrane tension gradient in rapidly moving cells, Biophys. J. 108 (2015) 1599−1603.

[37] D. Bray, M.D. Levin, C.J. Morton-Firth, Receptor clustering as a cellular mechanism to control sensitivity, Nature 393 (1998) 85−88.

[38] M.C. Mendoza, M. Vilela, J.E. Juarez, J. Blenis, G. Danuser, ERK reinforces actin polymerization to power persistent edge protrusion during motility, Sci. Signal. 8 (2015) ra47.

https://doi.org/10.1016/j.heliyon.2018.e00819

[39] S.K. Shenoy, et al., beta-Arrestin-dependent, G protein-independent ERK1/2 activation by the beta2 adrenergic receptor, J. Biol. Chem. 281 (2006) 1261−1273.

[40] G. Scita, P.P. Di Fiore, The endocytic matrix, Nature 463 (2010) 464−473.

[41] E. Marco, R. Wedlich-Soldner, R. Li, S.J. Altschuler, L.F. Wu, Endocytosis optimizes the dynamic localization of membrane proteins that regulate cortical polarity, Cell 129 (2007) 411−422.

[42] A.J. Lomakin, et al., Competition for actin between two distinct F-actin networks defines a bistable switch for cell polarization, Nat. Cell Biol. 17 (2015) 1435−1445.

https://doi.org/10.1016/j.heliyon.2018.e00819